Supporting Information

Unlocking azobenzene isomerization mechanisms via an LLM agent-driven workflow integrating simulation, experiment, and machine learning

Yixi Shen[1,†], Ledu Wang[1,†], Yan Huang[1,†,*], Xiaolong Zhang[1,†], Meng Huang[1], Huirong Li[1], Jing He[1], Aoran Cai[1], Yang Wang[1], Pieter E. S. Smith[2], Jun Jiang[1,3,*], Zhuoying Zhu[1,*], & Linjiang Chen[1,*]

[1] State Key Laboratory of Precision and Intelligent Chemistry, Hefei National Research Center for Physical Sciences at the Microscale, School of Chemistry and Materials Science, University of Science and Technology of China, Hefei 230026, China
[2] Hefei JiShu Quantum Technology Co., Ltd., Hefei 230026, China
[3] Hefei National Laboratory, University of Science and Technology of China, Hefei 230026, China

† These authors contributed equally: Y.S., L.W., Y.H., and X.Z.

* Corresponding authors. E-mails: hyang@ustc.edu.cn (Y.H.), jiangj1@ustc.edu.cn (J.J.), zyzhuq@ustc.edu.cn (Z.Z.), linjiangchen@ustc.edu.cn (L.C.)

This file includes

Computational and data processing details
The machine learning model
Structural transformation and spectral analysis of bridged azobenzene and azobenzene
Known bridged azobenzene derivative molecules used for neural network training (Tables S1–S2)
Schematic of sliding window data processing (Fig. S1)
Attention mechanism prioritization of spectral regions (Figs. S2–S5 and Tables S3–S6)
Analysis of High-Weight Spectral Regions (Figs. S6 and Tables S7)
Synthesis of bridged azobenzene and verification by ^{1}H NMR spectroscopy (Figs. S7-S8)
The experimental 1H NMR spectrum and MS spectrum of bridged azobenzene (Figs. S9-S10)
The experimental and theoretical infrared and Raman spectra of bridged azobenzene (Figs. S11-S14)
Distribution of Pearson correlation coefficients between predicted dihedral angles of bridged azobenzene and illumination time across 50 tests (Fig. S15)
The experimental 1H NMR spectrum, infrared, and Raman spectra of azobenzene (Figs. S16-S18)
Distribution of Pearson correlation coefficients between predicted dihedral angles of azobenzene and illumination time across 50 tests (Fig. S19)
LLM dialogs
References

1. Computational and data processing details

1.1 *Ab initio* molecular dynamics and DFT calculations

Ab initio molecular dynamic (AIMD) simulation with the hybrid Gaussian plane wave (GPW)[1] scheme was performed using CP2K package to investigate the change of a dihedral angle for the bridging azobenzene system and other transfer systems. The quickstep method with a plane wave cutoff of 500 Ry and the Goedecker-Teter-Hutter pseudopotentials was employed to describe the rest core electrons. The PBE exchange-correlation functional[2] and the Grimme-D3 dispersion correction[3] were accounted for the exchange-correlation effects and the van-der-Waals interactions, respectively. The localized double ξ-valence-polarized (DZVP) basis set[4] was applied to expand the wave functions. In this work, we adopted metadynamics[5], and the reaction time scale was accelerated by adding a systematic biasing potential to describe the reaction mechanism, where the dihedral angle was chosen as the CV. AIMD simulations in the canonical ensemble (NVT) were carried out using a Nose-Hoover thermostat[6] to gain insight into its behavior. The simulation was run for a duration of 5 ps, with a step size of 0.5 fs. We selected approximately 500 steps, encompassing the complete transition of the molecule from the Z conformation to the E conformation. The infrared and Raman spectra of bridging azobenzene molecule and its derivatives were calculated using Gaussian 16 software and the B3LYP functional. The calculations employed the 6-31+G(d,p) basis set for the system.

1.2 Known bridged Azobenzene derivative molecules

Table S1. The following are the bridged Azobenzene derivative molecules that already exist in various literature sources, which are used for our network training.

Reference[8]	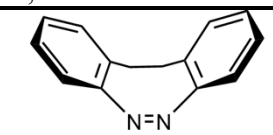	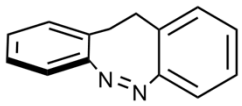
	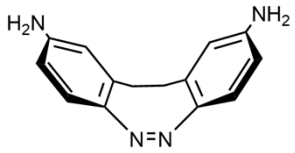	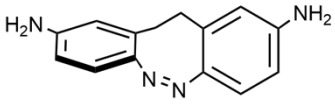
	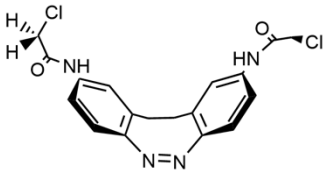	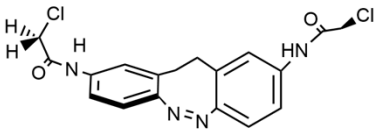
	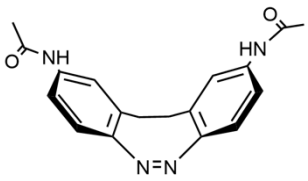	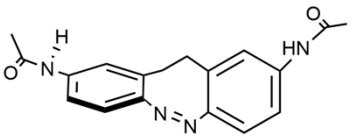
Reference[9]	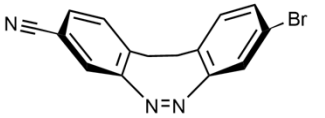	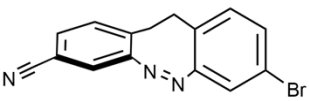
	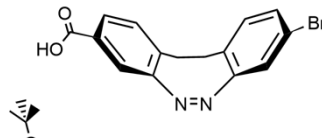	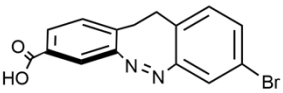
	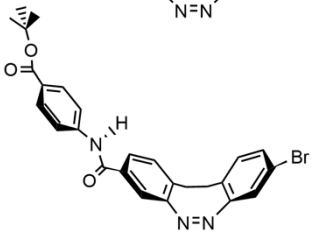	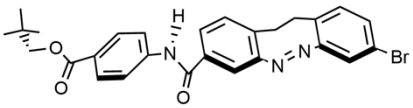
Reference[10]	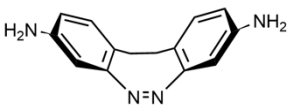	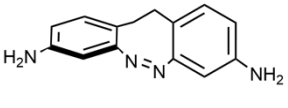

Reference[11]	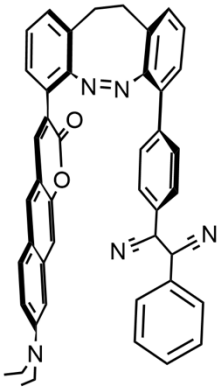	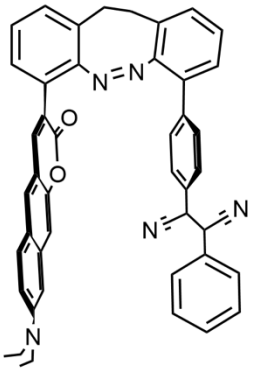
	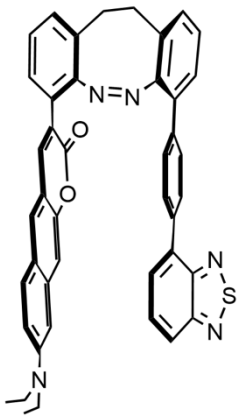	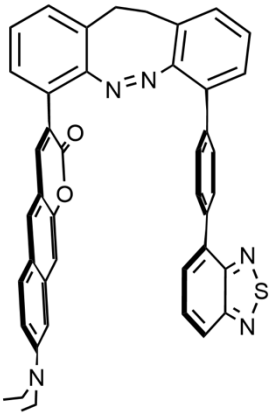
	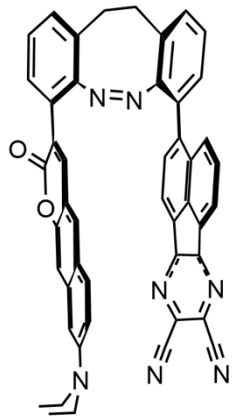	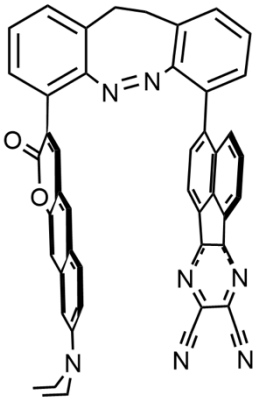

Table S2. The following are the bridged Azobenzene derivative molecules that already exist in the literature used for our Transfer learning.

Reference[12]	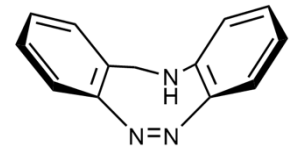	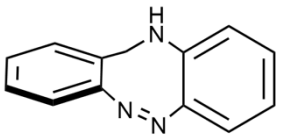
	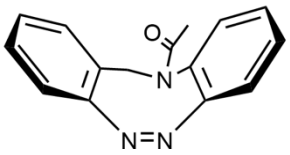	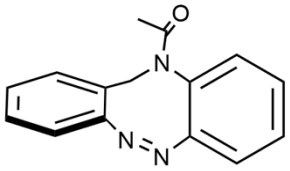

1.3 Data preprocessing

Calculated spectral lines were Lorentz broadened to construct the infrared (IR) and Raman spectra. Lorentz broadening of the spectral lines was performed using Multiwfn software[7]. The Lorentz function is

$$L(\omega) = \frac{FWHM}{2\pi} \frac{1}{(\omega - \omega_i)^2 + 0.25 \times FWHM^2} ,$$

where ω is the abscissa of the spectrum, and FWHM is the full width at half maximum, which was set to 8 cm^{-1}. The IR and Raman spectra were calculated for a spectral window of 0 to 4000 cm^{-1}, and 4000 intensities were calculated (or artificially sampled) at equal intervals of 1 cm^{-1}.

To train the machine learning models, the intensity ranges of the spectra were uniformly scaled to [0, 1] as follows:

$$x^* = \frac{x - \min(x)}{\max(x) - \min(x)} .$$

The sliding window technique is commonly used in sequential data processing and computation. Here, the average effect of zeroing 16 consecutive intensities of the spectrum on our model's dihedral angle prediction was calculated using a sliding window method. The sliding window method is based on the concept of a window which is moved from the starting position of the sequence towards the ending position of the sequence in fixed step sizes until it covers the entire sequence or meets specific stop conditions. Here, the sequence is a spectrum spanning 0–4000 cm^{-1}, with a window size of 16 cm^{-1} and a step size of 4 cm^{-1}. The following is a schematic diagram of the sliding window method employed.

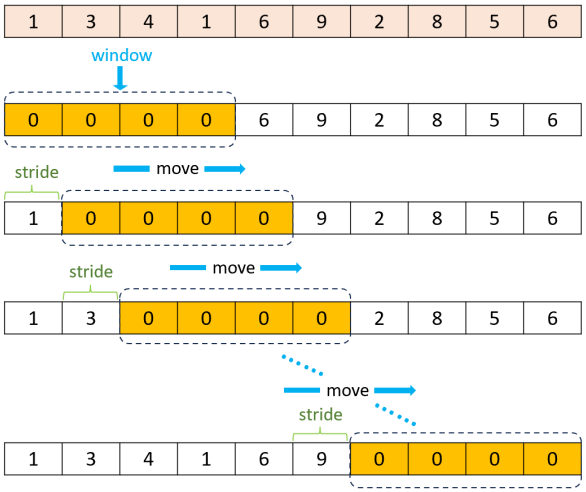

Fig. S1. Schematic diagram of the sliding window technique.

2. The machine learning model

2.1 Network architecture and parameter settings

All machine learning algorithms were implemented by PyTorch. The one-dimensional Convolutional neural network we use consists of three convolutional units, two attention units, and two fully connected units. Each convolution unit consists of convolution layer, batch normalization layer, Activation function and pooling layer. The size and step size of the convolutional kernels for the three convolutional units are (9, 1), (7, 1), and (3, 1), respectively. The number of input and output channels for the three convolutional units is (2, 32), (32, 64), and (64, 128), respectively. The input channels of the two attention units connected in the middle are 32 and 64, respectively. The two fully connected units are composed of convolution layer, Activation function and dropout. During the training process, in order to prevent data overfitting, the dropout designed here is 0.5. The Activation function in the network uses ReLU, and the optimizer uses Adam. When training the network, the Learning rate is initially set to 0.001. In order to speed up convergence, improve model performance, and reduce the workload of manual parameter adjustment, we use the ReduceLROnPlateau scheduler to adaptively adjust the Learning rate of the model. During the fine tuning of Transfer learning, the network framework remains unchanged, the parameters of the first two convolution units and the first attention unit are frozen, and then 100 retraining sessions are conducted, with an initial learning rate of 0.01.

2.2 Neural network attention weight distribution

In this article, we analyze the weight distribution of the last attention layer in the neural network and show the position with the highest weight in Fig. 3 of the main text. In fact, all weights are distributed within the spectral range of 0-4000cm^{-1}, and the sum of all weights is 1. We have drawn a distribution map of the 5 positions with the highest weight for each of the 4 molecules in the main text to illustrate.

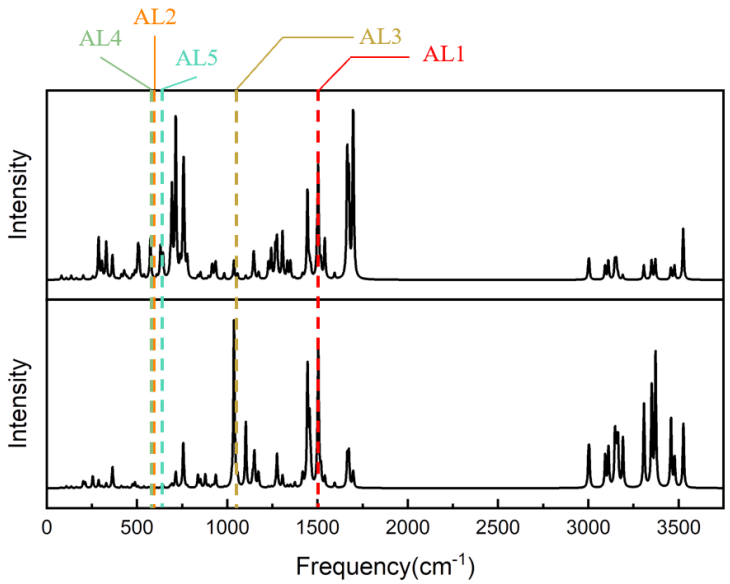

Fig. S2. Schematic diagram of the AL1-5 positions of the attention network weights of molecules in Fig. 3a in the main text.

Table S3. The specific positions and weights of AL1-5 in Fig. S2.

	Location(cm^{-1})	Weight
AL1	1499.5	0.783
AL2	595.5	0.024
AL3	1035.5	0.014
AL4	587.5	0.008
AL5	659.5	0.007

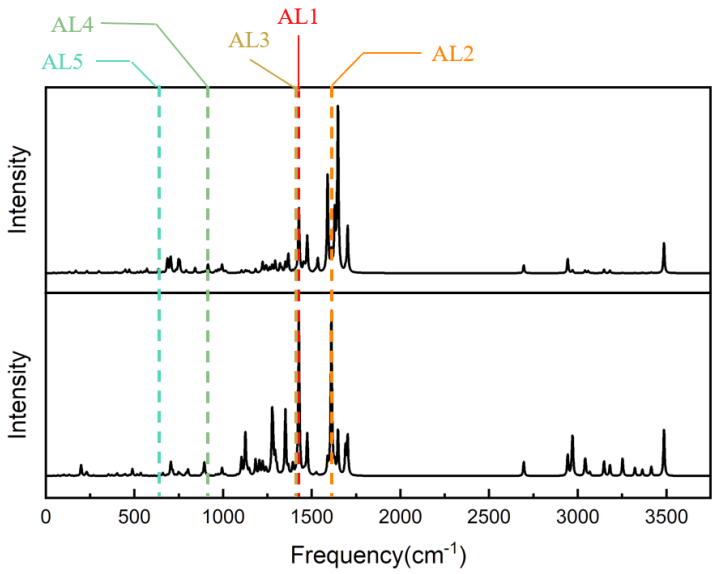

Fig. S3. Schematic diagram of the AL 1-5 positions of the attention network weights of molecules in Fig. 3b in the main text.

Table S4. The specific positions and weights of AL1-5 in Fig. S3.

	Location(cm^{-1})	Weight
AL1	1427.5	0.746
AL2	1611.5	0.034
AL3	1419.5	0.014
AL4	923.5	0.010
AL5	635.5	0.005

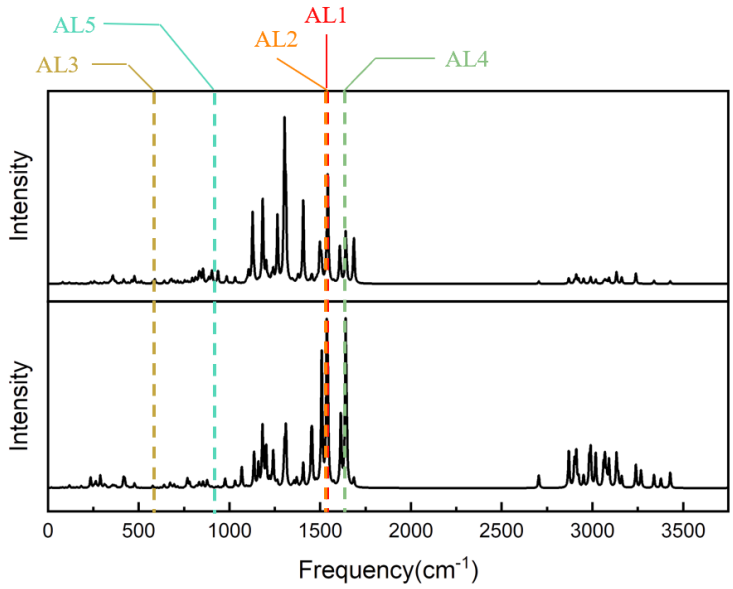

Fig. S4. Schematic diagram of the AL 1-5 positions of the attention network weights of molecules in Fig. 3c in the main text.

Table S5. The specific positions and weights of AL1-5 in Fig. S4.

	Location(cm^{-1})	Weight
AL1	1539.5	0.651
AL2	1531.5	0.079
AL3	595.5	0.020
AL4	1643.5	0.012
AL5	915.5	0.008

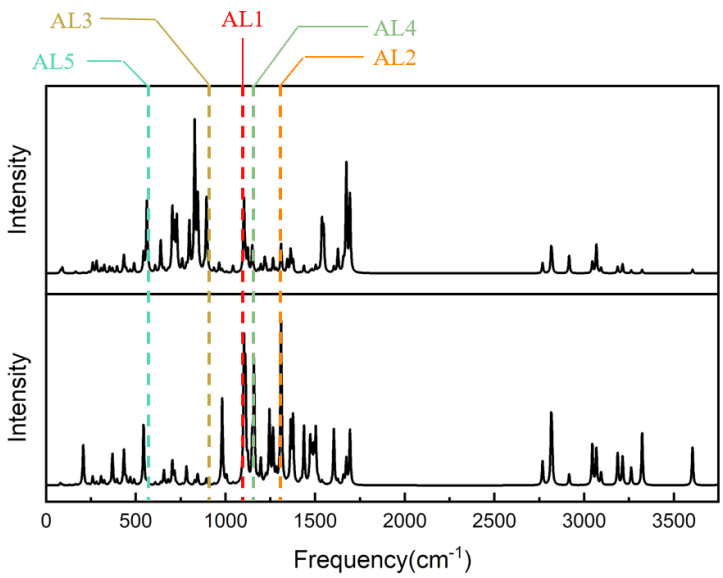

Fig. S5. Schematic diagram of the AL 1-5 positions of the attention network weights of molecules in Fig. 3d in the main text.

Table S6. The specific positions and weights of AL1-5 in Fig. S5.

	Location(cm^{-1})	Weight
AL1	1099.5	0.723
AL2	1307.5	0.034
AL3	915.5	0.024
AL4	1163.5	0.009
AL5	587.5	0.008

2.3 Analysis of High-Weight Spectral Regions

To elucidate the chemical basis of the attention mechanism when the highest-weight spectral region (AL1) deviates from the N=N stretching vibration—as observed in the TOP1 analysis ($r = 0.64$, Fig. 4a of the main text)—we performed a systematic analysis of the 40 cases with the largest discrepancies (outlined by purple dashed lines in Figure. 4e).

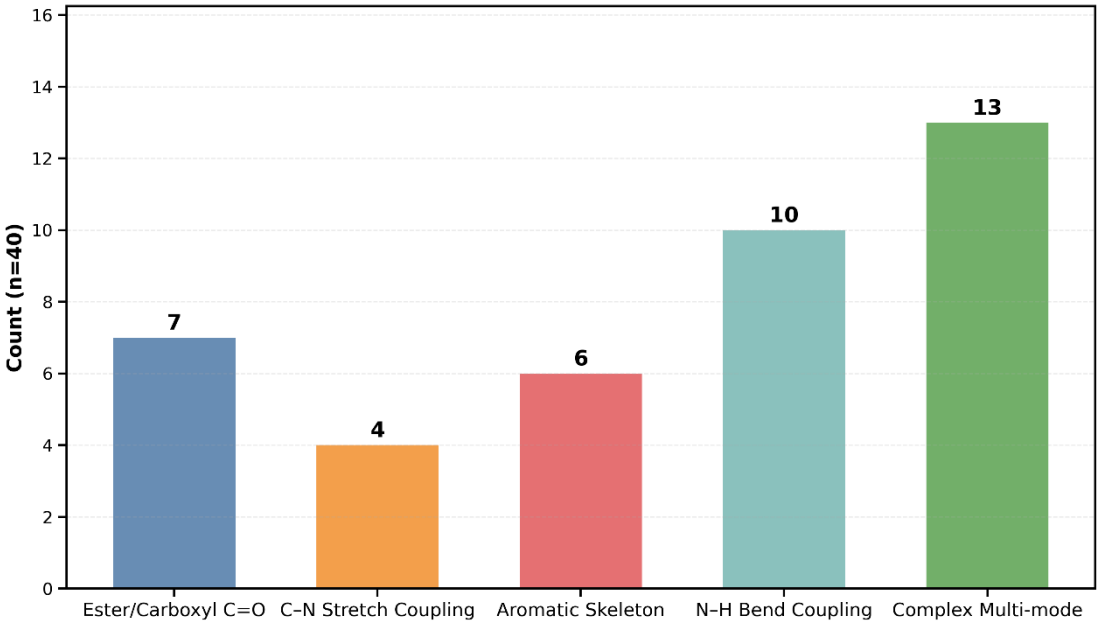

Fig. S6: Statistical distribution of vibrational modes at the model's highest-weight regions (based on 40 cases with the largest deviation in attention from the N=N stretching peak). The vibrational modes are categorized as follows: ester/carboxyl C=O stretching, C–N stretch coupling, aromatic skeleton vibrations (including ring breathing and asymmetric stretching), modes dominated by N–H bending and coupled with aromatic ring skeletal vibrations, and complex multi-mode coupling involving collective motions of multiple bonds/rings. This distribution demonstrates that when the N=N stretch is not the optimal predictive indicator in a specific molecular context, the model's attention systematically focuses on the aforementioned vibration modes with clear chemical interpretations.

Statistical Overview.

A categorical analysis of the vibrational modes corresponding to these anomalous AL1 regions is presented in Fig. S6. The distribution reveals that the model's attention systematically shifts to several chemically interpretable classes of vibrations: complex multi-mode coupling, C–N stretching coupled with aromatic motions, aromatic skeleton vibrations (including ring breathing), modes dominated by N–H bending, and ester/carboxyl C=O stretching. This pattern demonstrates that the "anomalous" attention is not random noise but follows chemically meaningful trends.

Representative Case Studies and Mode Assignments.

We selected four representative molecules for detailed vibrational mode assignment to illustra

te the physicochemical link between the prioritized spectral feature and the target C–N=N–C dihedral angle (φ). The results are summarized in Table S7.

Table. S7: Vibrational mode assignment and chemical interpretation for four representative cases where the model's highest attention deviates from the N=N stretching region.

Molecular structure	Location (cm-1)	Vibrational mode assignment	Chemical interpretation: link to φ and context for model's selection
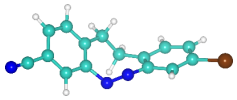	891.5	C–N stretch coupled with aromatic C–H out-of-plane bend.	The essence of this vibrational mode is the concerted out-of-plane twisting motion of the benzene ring and the C–N bond. Serving as the reaction coordinate for the φ angle, it exhibits exceptionally high sensitivity to changes in φ.
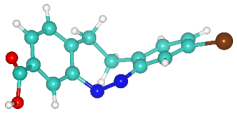	1083.5	C–N stretch-dominated mode with in-plane ring breathing.	The core of this vibrational mode is the stretching of the key C–N bond that constitutes the CNNC dihedral angle. It directly reports the local tensile strain induced in this bond by the distortion of the φ angle. Consequently, its frequency provides a clear and specific readout of the local stress state.
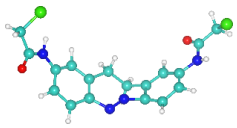	1587.5	N–H bending vibration coupled with the skeletal vibration of the adjacent benzene ring.	The φ angle governs the delocalization extent of the π-electrons in the N=N bond, thereby affecting the electron density at the peripheral N atom. The N–H bending frequency is highly sensitive to such long-range electronic changes, resulting in a substantial shift that correlates systematically with φ.
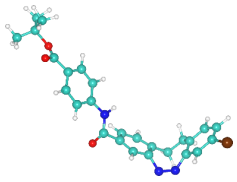	1715.5	C=O stretching vibration of the ester group coupled with the skeletal stretching vibration of the adjacent benzene ring.	The φ angle modulates the electron density of the benzene ring by tuning the overall conjugation efficiency of the molecule. This change is transmitted through chemical bonds, ultimately affecting the force constant of the C=O bond. The intense and sharp C=O band provides a cleaner and more isolated spectral signature, which can reliably report the long-range electronic changes dictated by the φ angle.

1. **C–N Coupling with Aromatic Out-of-Plane Bend (891.5 cm^{-1}):** The mode involves concerted out-of-plane motion of the C–N bond and the adjacent benzene ring, which directly correlates with the twisting coordinate of φ, granting it high sensitivity to co nformational changes.

2. **C–N Stretch-Dominated Mode with Ring Breathing (1083.5 cm^{-1}):** The stretching of the C–N bond, a constituent of the CNNC dihedral, directly reports local tensile str ain induced by φ distortion, providing a specific spectral readout of the local stress sta te.
3. **N–H Bending Coupled with Aromatic Skeletal Vibration (1587.5 cm^{-1}):** The φ an gle modulates π-electron delocalization in the N=N bond, affecting electron density at the peripheral N atom. The N–H bending frequency is sensitive to such long-range el ectronic changes, resulting in systematic shifts correlated with φ.
4. **Ester C=O Stretch Coupled with Aromatic Stretching (1715.5 cm^{-1}):** Changes in φ alter the conjugation efficiency of the molecule, thereby modulating electron densit y of the benzene ring. This effect propagates through bonds to influence the C=O forc e constant, making the intense and isolated C=O band a reliable reporter of long-rang e electronic changes dictated by φ.

Implications for Model Interpretation.

This analysis confirms two key aspects of the ATT-CNN model:

- **Context-Dependent Feature Selection:** The attention mechanism does not rigidly fi xate on the N=N stretch as a universal descriptor. Instead, it dynamically identifies th e spectral feature that exhibits the strongest correlation with φ and the highest discrim inative power within a given molecular environment—which could be the N=N stretc h, a C–N coupled mode, a C=O stretch, or another chemically relevant vibration.
- **Basis for Holistic Spectral Evaluation:** The fact that these "anomalous" AL1 region s correspond to physically meaningful vibrations explains why the model maintains hi gh predictive accuracy even when the N=N stretch is not the primary focus. It demons trates the model's capacity to leverage multiple, complementary spectral probes that c ollectively encode conformational information.

Together, the statistical distribution (Fig. S6) and the detailed mode assignments (Table S7) v alidate that the attention mechanism learns and utilizes a complex, multifaceted mapping betw een spectral regions and molecular structure. This capability underpins the model's robustness and its chemically interpretable decision-making process.

3. Structural Transformation and Spectral Analysis of Bridged Azobenzene and Azobenzene

Materials

Unless otherwise noted, all starting materials, reagents, and solvents were obtained from commercial suppliers and were used without further purification. Analytical thin layer chromatography (TLC) was performed on glass silica gel plates; visualization of products was performed with a handheld UV lamp. All aqueous solutions were prepared with deionized distilled water obtained from a Milli-Q water-purifying system (18 MΩ cm).

Synthesis of Bridged Azobenzene

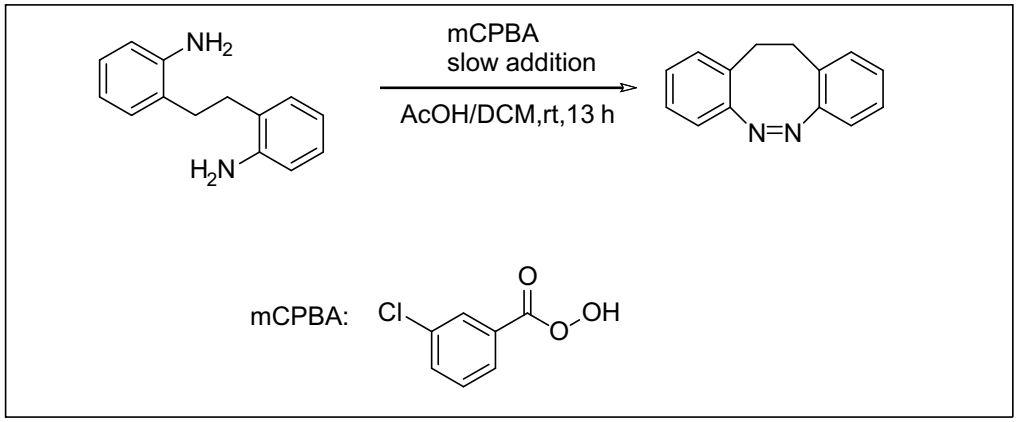

Fig. S7. Synthesis of Bridged Azobenzene.

The target compound were synthesized according to the literature procedure[13]. A freshly prepared and titrated (0.57 – 0.62 M) solution of mCPBA (500 µmol, 2.0 eq.) in acetic acid was added by syringe pump within a period of 12 hours under rapid stirring to a solution of a 2,2'-ethylenedianiline substrate (250 µmol, 1.0 eq.) in acetic acid/dichloromethane = 1/3 (6.25 mL). After the complete addition of the mCPBA solution, the mixture was stirred for at least one more hour. The solvent was then removed under reduced pressure, the residue taken up in ethyl acetate (10 mL) and washed with saturated, aqueous sodium hydrogen carbonate (2×5 mL), followed by saturated, aqueous sodium chloride (5 mL). The solution was dried over sodium sulfate, the solvent was removed under reduced pressure and the residue was purified by column chromatography (2% ethyl acetate in petroleum ether) to afford the target compound (11mg ,21%) as a yellow solid. The 1HNMR spectrum of the compound are in good agreement with the reported literature[13].

1H-NMR (400 MHz, CDCl3): 7.13 (ddd, J = 7.6, 7.0, 1.8 Hz, 2H), 7.01 (m, 4H), 6.83 (d, J = 7.6 Hz, 2H), 3.09 – 2.68 (m, 4H).

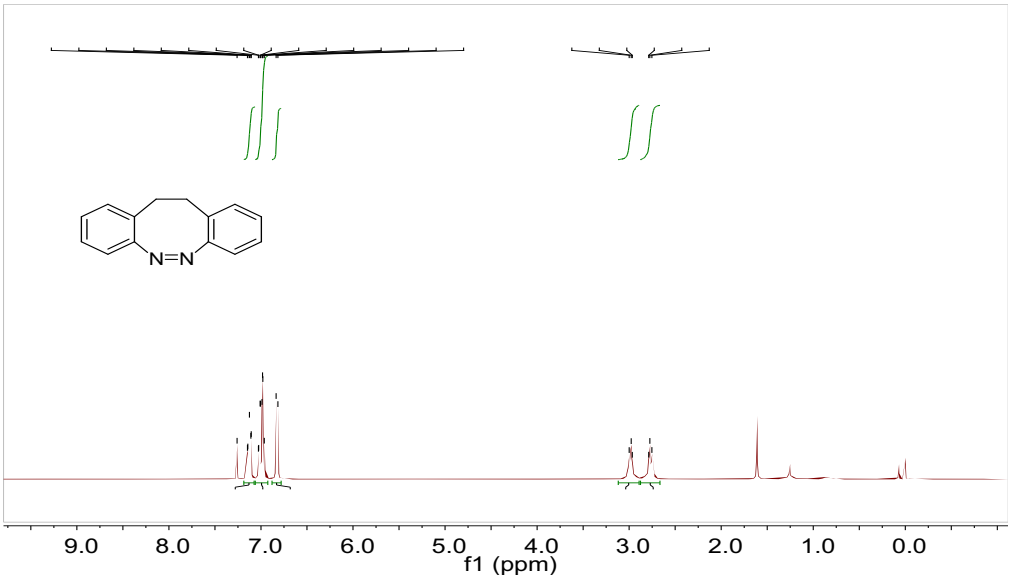

Fig. S8. ^{1}H NMR spectrum of bridged azobenzene in $CDCl_3$.

Source of Azobenzene

Azobenzene (CAS: 103-33-3) was purchased from Sigma-Aldrich.

Nuclear Magnetic Resonance (NMR) Spectroscopy

^{1}H NMR spectra were recorded using a Magritek Spinsolve 60 spectrometer. All spectra were acquired at 25°C, with deuterated solvents including chloroform-d ($CDCl_3$, 99.8% D) and dimethyl sulfoxide-d_6 (DMSO-d_6, 99.9% D).

Infrared (IR) Spectroscopy

IR spectra were recorded using a Thermo Scientific™ Nicolet™ iS20 FTIR spectrometer. Data were presented in wavenumbers (cm^{-1}) with a measurement range of 650–4000 cm^{-1}. Sample measurements were conducted in two ways: (1) after phototreatment in dichloromethane solution, followed by solvent evaporation to form a thin film for measurement; (2) in a thermostatic device, maintaining the sample in dichloromethane solution for measurement.

Raman Spectroscopy

Raman spectra were recorded using a LabRAM HR Evolution spectrometer. Data were presented in wavenumbers (cm^{-1}) with a measurement range of 650–4000 cm^{-1}. The sample measurement methods were identical to those for IR spectroscopy.

Structural Transformation and Spectral Analysis of Bridged Azobenzene under Light Irradiation

We irradiated the b-Azo molecule (298 K, DMSO-d_6 solution, 24 mM) with 400 nm light and measured the ^{1}H NMR spectra after different irradiation durations until the total irradiation time reached 2130 seconds (Fig. S9). It was observed that after a cumulative irradiation of 600 seconds, the ^{1}H NMR spectra no longer exhibited significant changes. Additionally, GC and MS analyses confirmed that the compound underwent only the cis-to-trans isomerization during irradiation, with no decomposition products detected (Fig. S10). Therefore, for the infrared and Raman spectral measurements, we selected an irradiation time range of 0–600 seconds. During this period, we recorded the changes in the infrared and Raman spectra at different irradiation times (at 60-second intervals), successfully capturing the transition of the b-Azo molecule from the Z configuration to the E configuration. Additionally, a detailed analysis of the spectral features of b-Azo at different irradiation times was conducted.

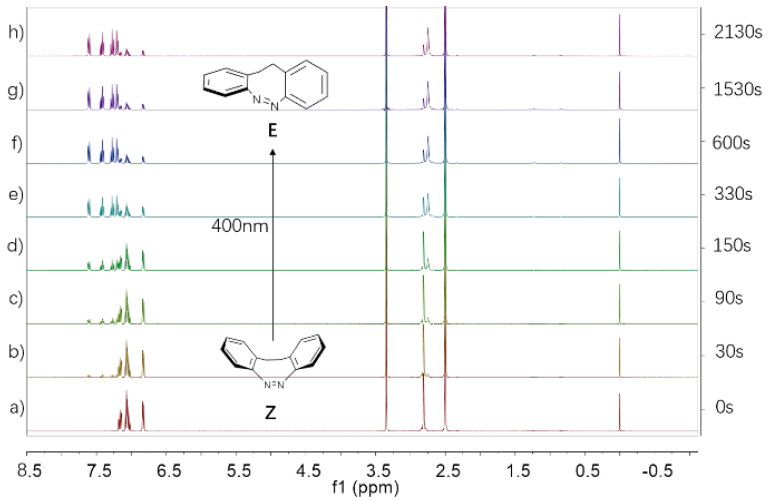

Fig. S9. ^{1}H NMR spectrum of molecule b-Azo(25°C, 24 mM in DMSO-d6) under Xe lamp equipped with 400 nm cut-off filter at different times a) 0; b) 30s; c) 90s; d) 150s; e) 330s; f) 600s; g) 1530s; h) 2130s.

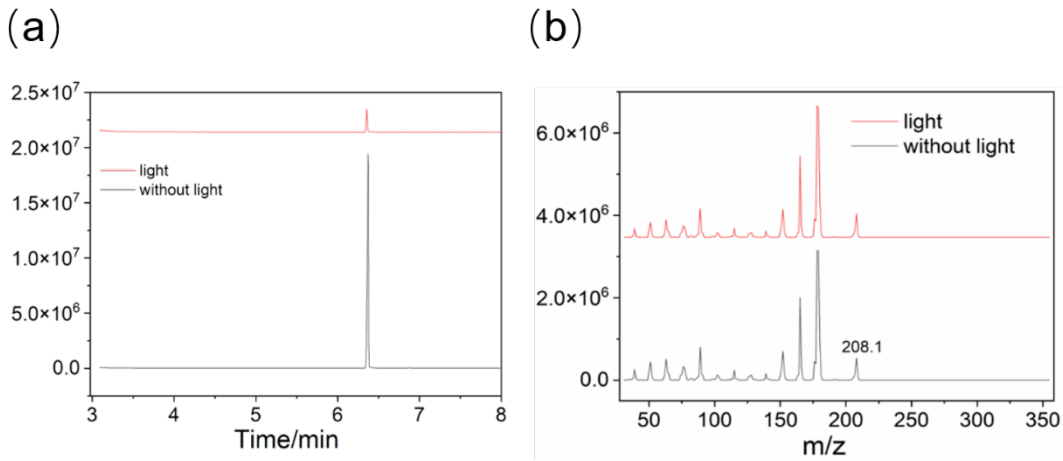

Fig. S10. (a) shows the GC spectrum of the b-Azo molecule in EA before irradiation (black line) and after 30 minutes of 400 nm light irradiation (red line); (b) presents the corresponding mass spectrum (MS) under the same conditions. The MS results indicate that during the irradiation process, the compound undergoes only the cis-to-trans isomerization, with no detectable decomposition products.

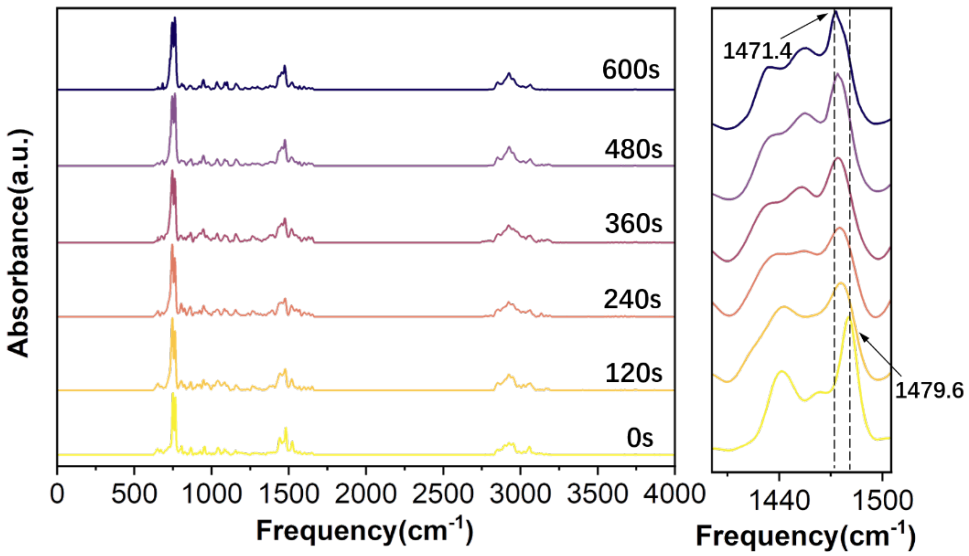

Fig. S11. Experimental infrared spectra of the b-Azo molecule after 0–600 seconds of 400 nm light irradiation. The figure presents spectral changes at different time points. The inset on the right magnifies the absorption peak near 1470 cm^{-1}, highlighting the observed redshift phenomenon. This indicates that as the irradiation time increases, structural changes occur in the b-Azo molecule, leading to a shift in the position of this absorption peak in the infrared spectrum.

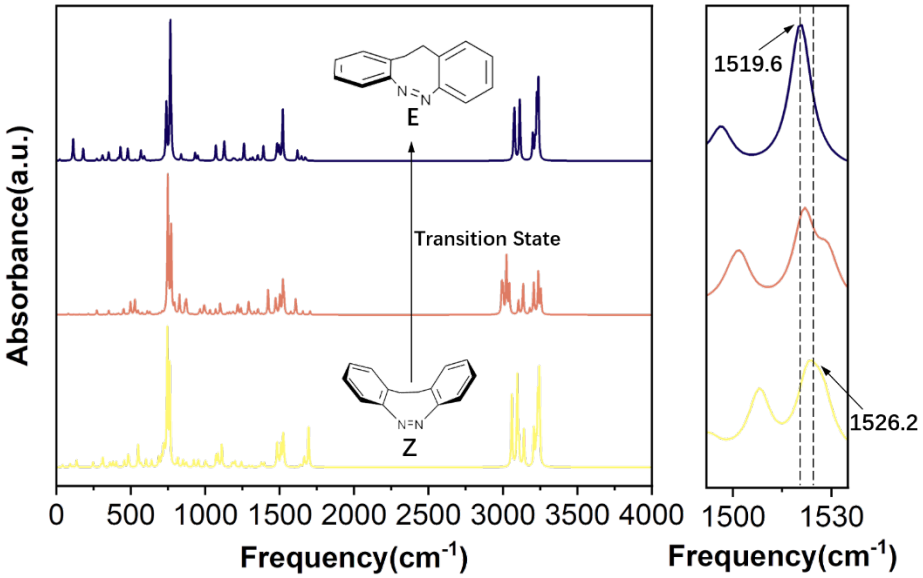

Fig. S12. Theoretical infrared spectra of the b-Azo molecule in the Z configuration, E configuration, and transition state. The inset on the right magnifies the absorption peak near 1520 cm^{-1}, highlighting the observed redshift phenomenon.

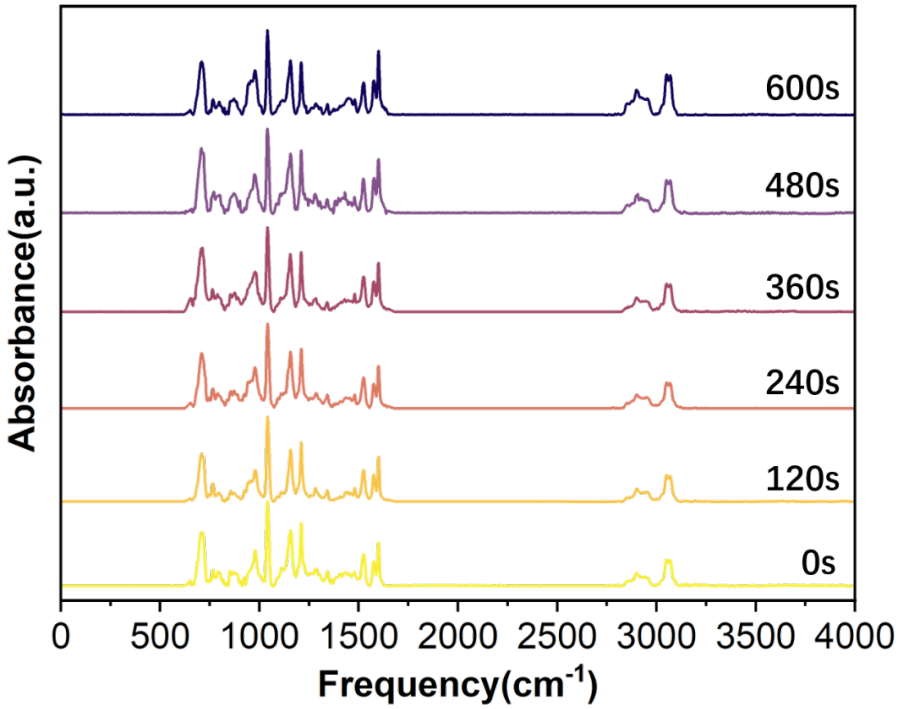

Fig. S13. Experimental Raman spectra of the b-Azo molecule after 0-600 seconds of 400 nm light irradiation, showing spectral changes at different time points.

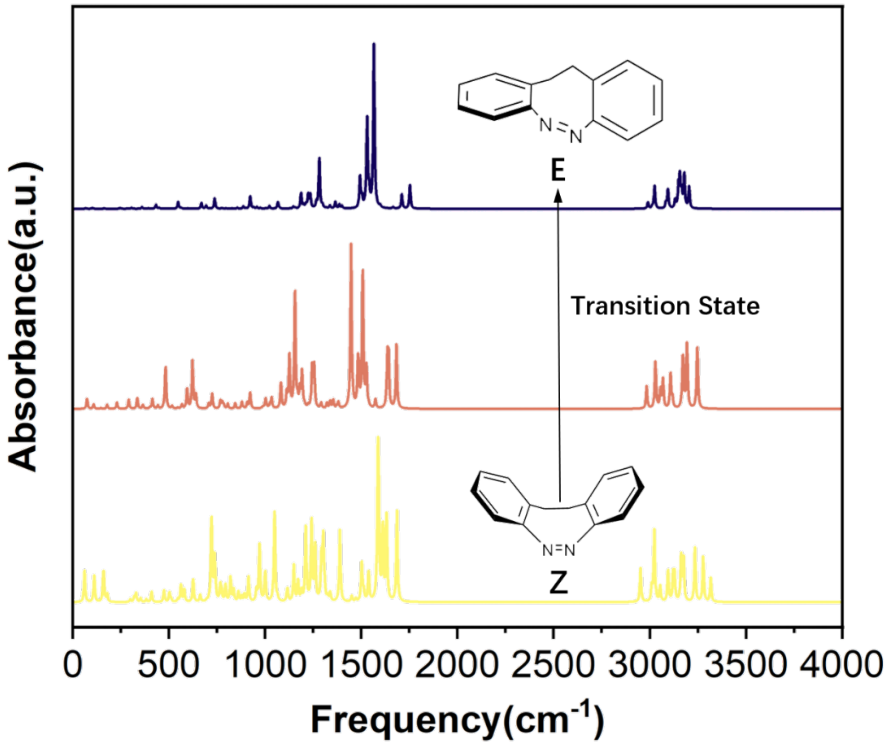

Fig. S14. Theoretically calculated Raman spectra of the b-Azo molecule in the Z configuration, E configuration, and transition state.

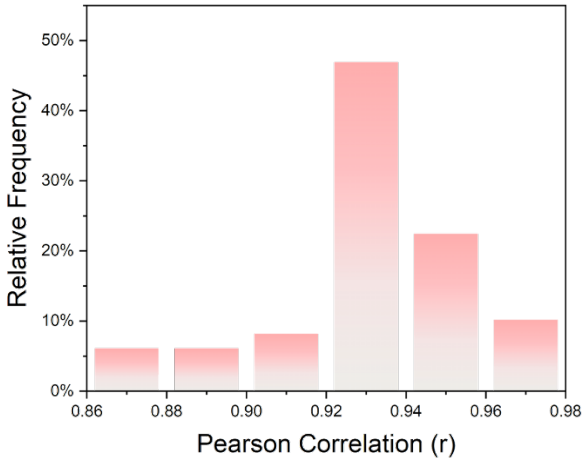

Fig. S15. The 19 experimental datasets were randomly divided into training and test sets (9:10), and 50 tests were conducted. The figure illustrates the distribution of the Pearson correlation coefficient (r) between the predicted dihedral angle and illumination time across these 50 tests. The x-axis represents the Pearson correlation coefficient (r), ranging from 0.86 to 0.98, while the y-axis denotes the relative frequency, indicating the occurrence frequency within each correlation coefficient range. The average Pearson correlation coefficient across the 50 tests is 0.9347.

Structural Transformation and Spectral Analysis of Azobenzene under Constant-Temperature Heating

To investigate the spectral changes during the configurational transformation of azobenzene under heating conditions, we first induced its isomerization using 350 nm xenon lamp irradiation. The resulting mixture was then purified through column chromatography, yielding high-purity cis-azobenzene.

We then used a constant-temperature heating device to heat the azobenzene molecules (70°C, dichloromethane solution, 26.2 mM) and measured the ^{1}H NMR spectra at different heating time points, until the heating time reached 100 minutes and no further significant changes were observed in the ^{1}H NMR spectra (Fig. S16). Therefore, for the infrared and Raman spectral measurements, we selected a heating time range of 0-100 minutes. During this period, we recorded the changes in the infrared and Raman spectra at different heating times (with 5-minute intervals), capturing the process of the azobenzene molecule transitioning from the Z configuration to the E configuration (Fig. S17 ,S18).

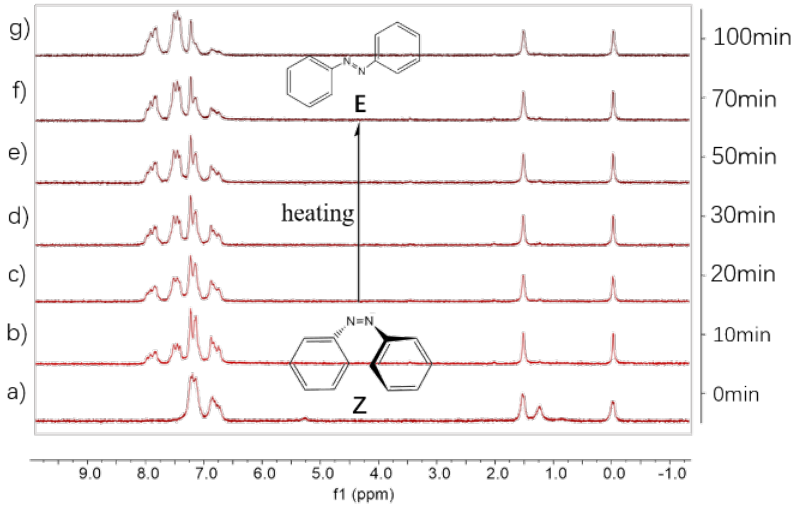

Fig. S16. ^{1}H NMR spectra of azobenzene at different heating times during constant-temperature heating at 70°C (60 MHz, $CDCl_3$, 298 K, 26.2 mM), as follows: a) 0 minutes; b) 10 minutes; c) 20 minutes; d) 30 minutes; e) 50 minutes; f) 70 minutes; g) 100 minutes.

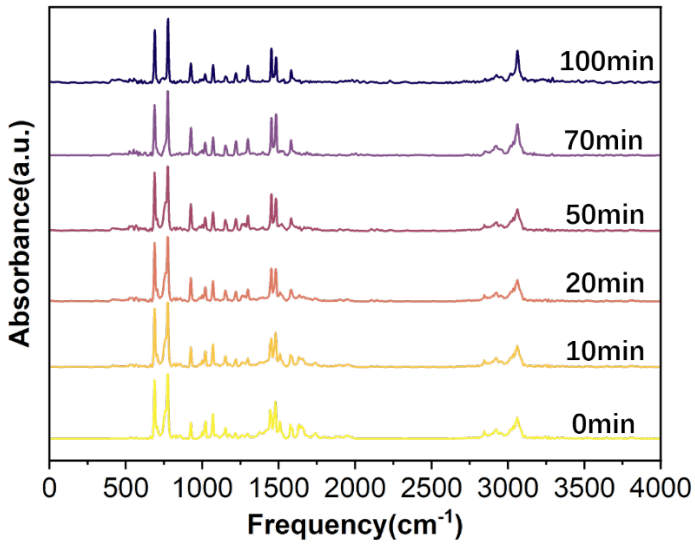

Fig. S17. Infrared spectra of the Azo molecule at different heating times during a 100-minute constant-temperature heating process at 70°C.

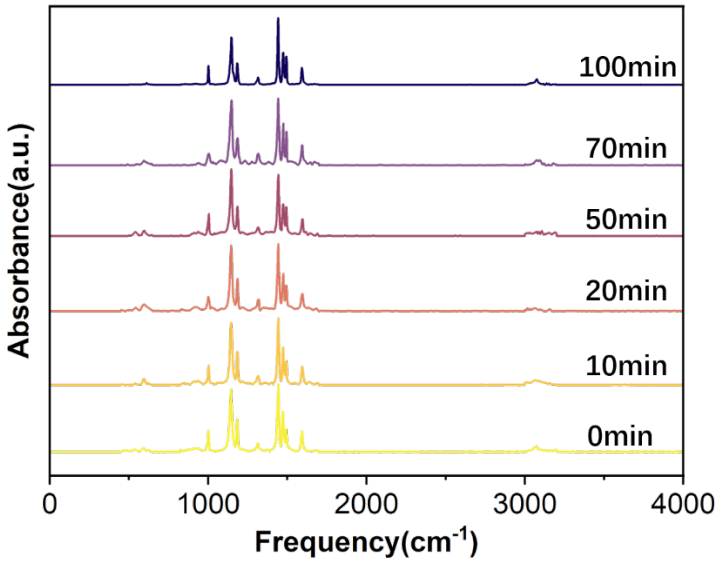

Fig. S18. Raman spectra of the Azo molecule at different heating times during a 100-minute constant-temperature heating process at 70°C.

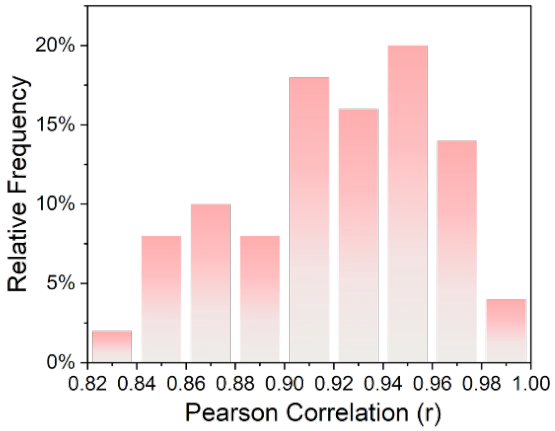

Fig. S19. The 20 experimental datasets were randomly divided into training and testing sets (in a 10:10 ratio), and 50 tests were conducted. The figure shows the distribution of the Pearson correlation coefficient (r) between the neural network-predicted dihedral angle and illumination time across these 50 tests. The x-axis represents the Pearson correlation coefficient (r), ranging from 0.82 to 1.00, while the y-axis denotes the relative frequency, indicating the occurrence frequency within each correlation coefficient range. The average Pearson correlation coefficient across the 50 tests is 0.9221.

4. LLM Dialogues

GraphRAG Knowledge Graph Parameters

LLM and Embedding Models: Text generation and entity extraction utilized the deepseek-chat (at the time DeepSeek V3, version 0528) model with the cl100k_base tokenizer and structured JSON output enabled. Vector embeddings were generated using OpenAI's text-embedding-3-small model (1536 dimensions) and stored in a local LanceDB vector database.

Indexing and Chunking: Source documents were processed using a sliding window strategy with a chunk size of 1200 tokens and an overlap of 100 tokens to maintain context continuity.

Information Extraction (Schema): Entity extraction was governed by the default GraphRAG entity prompt. The system used a "max gleanings" setting of 1 to ensure coverage. Claim extraction and graph embeddings (Node2vec) were disabled for this implementation.

Community Detection and Clustering: The hierarchical community structure was built using a maximum cluster size of 10. Community summaries were generated using the default community_report.txt prompt, with a maximum input context of 8000 tokens and a generated report limit of 2000 tokens.

Querying: The system was configured to support both Local Search (neighborhood-specific) and Global Search (map-reduce across community summaries) using the default GraphRAG system prompts.

GraphRAG Knowledge Query

Global Search Prompt:

From the knowledge base, please note some key methods for investigating the Z-E isomerism of azobenzene derivatives.

Response:

Key Methods for Investigating Z-E Isomerism in Azobenzene Derivatives

The study of Z-E isomerism in azobenzene derivatives employs a diverse array of experimental and computational techniques to elucidate structural dynamics, electronic transitions, and photochemical behavior. Below are the most pivotal methods, categorized by their approach.

Computational & Theoretical Methods

Complete Active Space Self-Consistent Field (CASSCF)

A high-level quantum chemistry method essential for studying electronic structures, excited-state potential energy surfaces, and nonadiabatic dynamics. It provides a balanced representation of multiple electronic states [Data: Reports (1115, 503, 434, +more)].

Variants like CASSCF(6,5)/6-31G and CASSCF(10,8)/6-31G* are used for dynamic simulations and conical intersection analysis [Data: Reports (597, 1117)].

Time-Dependent Density Functional Theory (TD-DFT)

Critical for calculating excitation energies, charge distributions, and UV-vis absorption spectra. Implementations like CAM-B3LYP/6-31G(D) enhance accuracy for excited-state properties [Data: Reports (1097, 1099, 1116, 1096, +more)].

Nonadiabatic Molecular Dynamics (NAMD) & Surface Hopping

Simulates transitions between electronic states during photoisomerization, incorporating methods like Tully's fewest-switches algorithm and Zhu-Nakamura theory [Data: Reports (855, 853, 1106, 508, +more)].

Restricted Open-shell Kohn-Sham (ROKS) & CASPT2

ROKS offers comparable accuracy to CASPT2 (within ~0.1 eV) for excited-state energy profiles [Data: Reports (1128)].

CASPT2//CASSCF/6-31G* is used for vertical transition analysis [Data: Reports (547, 1117)].

Ab Initio Molecular Dynamics (AIMD) & QM/MM

Combines quantum mechanics with molecular mechanics to model solvent effects and bulk-material behavior [Data: Reports (665, 529, 1105)].

Spectroscopic & Experimental Techniques

UV-Vis Spectroscopy

Measures absorption spectra and monitors photoisomerization kinetics, including ground-state cis-trans back-conversion [Data: Reports (1037, 735, 677, +more)].

Ultrafast Spectroscopy

Tools like sub-5-fs visible pulsed lasers and time-resolved Raman spectroscopy capture femtosecond-scale dynamics [Data: Reports (600, 975, 633, +more)].

Resonance Raman Spectroscopy

Probes vibrational modes and excited-state structures during isomerization [Data: Reports (1074, 439, 1073, +more)].

X-ray Crystallography & Diffraction

Confirms molecular conformations (e.g., Z1/Z2 isomers) and lamellar periodicity changes [Data: Reports (880, 1034, 1031)].

Fluorescence & Time-Resolved Techniques

Tracks excited-state decay and photophysical properties [Data: Reports (589, 1108, 536)].

Key Insights & Mechanisms

Electronic States: The S1 (nπ)* and S2 (ππ)* states mediate isomerization, with conical intersections (CI) enabling non-radiative decay [Data: Reports (650, 653, 672, +more)].

Photoisomerization Pathways:

E→Z (quantum yield: 0.46) and thermal isomerization are studied via Arrhenius plots and solvent effects [Data: Reports (672, 587, 699)].

Inversion vs. Rotation: Semiempirical methods (e.g., PM3, MNDO) distinguish these mechanisms [Data: Reports (205, 659)].

These methods collectively advance the understanding of azobenzene derivatives' photoresponsive behavior, with applications in materials science and photopharmacology.

Interactive Research Design
System Prompt:
Background
You are a chemical expert with expertise in the area of azobenzene derivatives research, especially in investigation of Z-E isomerism.
Knowledge
The “Response” section in the GraphRAG Global Query dialogue.
Answer
Your task is to propose an innovative research direction in the field of azobenzene derivatives, based on your specialized knowledge and the human's research goals. Please provide the rationale and thought process behind your proposal.
Interactive Dialogue:
User:
Our objectives: To conduct a systematic research on bridged azobenzenes with the bridge type similar to 11,12-Dihydrodibenzo[c,g][1,2]diazocine, develop a unified method that eludicates real-time status of molecules in a dynamic process of Z-E isomerization from observable information (e.g. vibrational spectrum).

LLM:
Proposed Research Direction:
Development of a Unified Ultrafast Vibrational Spectroscopy Platform Integrated with Machine Learning for Real-Time Tracking of Z-E Isomerization Dynamics in Bridged Azobenzenes
Rationale and Thought Process:

1. Addressing Core Objectives:
    - Your goal focuses on bridged azobenzenes (e.g., 11,12-Dihydrodibenzo[c,g][1,2]diazocine derivatives), which exhibit constrained geometries and unique isomerization pathways.
    - The need for a unified real-time method to track isomerization dynamics aligns with gaps in current techniques, which often lack spatiotemporal resolution or rely on indirect proxies (e.g., UV-Vis absorbance changes).
2. Leveraging Vibrational Spectroscopy:
    - Resonance Raman spectroscopy is ideal for probing structural changes during isomerization (as noted in Reports 63, 489, 490). It directly captures vibrational modes of the N=N bond and bridge deformations, providing a "molecular fingerprint" of Z/E states.
    - However, conventional Raman lacks the temporal resolution needed for ultrafast dynamics.
3. Innovative Integration:
    - Proposed Method: Combine femtosecond stimulated Raman spectroscopy (FSRS) with time-resolved infrared (TR-IR).
        - FSRS (ultrafast variant of Raman) offers ~50-fs time resolution and vibrational specificity, capturing transient intermediates (Report 699).
        - TR-IR monitors low-frequency modes (e.g., bridge flexing, N=N torsion) complementary to FSRS.
    - Why this pairing?
        - FSRS detects high-frequency modes (e.g., N=N stretch at 1400–1600 cm^{-1}) sensitive to electronic configurations.
        - TR-IR tracks low-frequency modes (<500 cm^{-1}) linked to bridge dynamics and inversion/rotation pathways.
        - Together, they cover the full vibrational spectrum critical for bridged systems.
4. Machine Learning for Real-Time Elucidation:
    - Challenge: Interpreting complex, overlapping spectral data in real time.
    - Solution: Train a neural network on simulated spectra from *nonadiabatic*

AIMD (Report 685) and *TD-DFT* (Report 695) for bridged azobenzenes.
        - Input: Time-resolved FSRS/TR-IR spectra.
        - Output: Real-time populations of Z/E states and intermediate structures.
    - Advantage: Unifies spectral data into a predictive model that quantifies isomerization kinetics and identifies hidden intermediates.
5. Validation and Universality:
    - Validate with ultrafast UV-Vis transient absorption (Report 128) to correlate electronic/vibrational changes.
    - Test universality across bridged derivatives:
        - Vary bridge rigidity (e.g., 8–12 membered rings).
        - Modify substituents (e.g., electron-donating/withdrawing groups).
    - Output: A generalized workflow adaptable to diverse azobenzene scaffolds.

Expected Outcomes:

- Real-Time Molecular "Movie": Visualize bond angle changes, bridge distortions, and inversion/rotation pathways with femtosecond resolution.
- Unified Kinetic Model: Extract rate constants ($k_{Z\rightarrow E}$, $k_{E\rightarrow Z}$) and identify solvent/temperature dependencies (Report 558).
- Design Rules: Predict how bridge geometry influences isomerization efficiency for photopharmacology or optoelectronics.

Why This Direction is Innovative:

- Beyond State-of-the-Art: Most studies use static techniques (NMR, XRD) or indirect methods (UV-Vis). This integrates ultrafast spectroscopy with AI for dynamic, atomistic insights.
- Bridging Theory/Experiment: Combines nonadiabatic simulations with experimental validation, addressing limitations of purely computational approaches.
- High Impact: Enables rational design of azobenzene-based molecular machines, sensors, or drug-delivery systems.

This approach directly addresses your objectives by transforming vibrational spectra into a real-time diagnostic tool for Z-E isomerization, with broad applicability to constrained azobenzene architectures.

User:

The idea of generating molecular "movie" from a femtosecond Raman experiment is promising, however, conducting such experiments are resource-extensive, and we would like to know if there are promising methods to generate such trajectories via simulations.

LLM:

Proposed Research Direction:

High-Fidelity Nonadiabatic Molecular Dynamics Simulations with Machine Learning-Accelerated Computational Spectroscopy for Predicting Real-Time Isomerization Trajectories in Bridged Azobenzenes

Rationale and Thought Process:

1. Addressing Resource Constraints:
    - While experimental ultrafast spectroscopy (e.g., FSRS) is powerful, its cost/time intensity can be mitigated by computational trajectory generation. Simulations offer atomic-resolution insights without instrumentation limitations.
    - Bridged azobenzene systems (e.g., 11,12-Dihydrodibenzo[c,g][1,2]diazocine) are ideal for simulation due to their constrained geometry, which simplifies potential energy surfaces (PES) and favors inversion-dominated pathways (Report 687).
2. Core Computational Strategy:
    - Nonadiabatic AIMD with Surface Hopping:
        - Use *time-dependent density functional theory (TD-DFT)* or *multireference methods (CASSCF)* for accurate excited-state dynamics (Reports 685, 695).

        - Implement trajectory surface hopping (TSH) to model non-radiative transitions between S_0/S_1 states during isomerization.
    - Key Advantage: Directly simulates femtosecond-scale bond rotation/inversion, electron redistribution, and bridge deformation (validated against Report 301).
3. Machine Learning Acceleration:
    - Challenge: Traditional AIMD is computationally prohibitive for long-timescale dynamics.
    - Solution:
        - Train a neural network potential (NNP) on high-level *ab initio* data (e.g., CCSD(T)/def2-TZVP) to replace quantum calculations during MD.
        - Employ active learning to iteratively refine the NNP using uncertainty quantification (e.g., querying configurations where prediction variance is high).
    - Expected Speedup: 10^3–10^6× faster than pure *ab initio* MD while maintaining chemical accuracy (validated by recent ML-accelerated photoisomerization studies).
4. Generating "Molecular Movies":
    - Workflow:

1. Simulate 500–1000 TSH trajectories initiated at Franck-Condon (FC) region after photoexcitation.
2. Extract time-resolved atomic coordinates (0.1-fs resolution).
3. Reconstruct vibrational spectra via:
        - DFT-based anharmonic frequency calculations for IR/Raman intensities.
        - Electric field autocorrelation for simulated FSRS signals.
    - Critical Output: Frame-by-frame visualization of:
        - N=N bond angle inversion (key for bridged systems).
        - Bridge strain evolution (e.g., dihedral changes in diazocine rings).
        - Charge transfer dynamics at conical intersections.
5. Validation and Experimental Synergy:
    - Low-Cost Benchmarking:
        - Compare simulated spectra with steady-state UV-Vis/Raman data (Report 489).
        - Validate kinetics against nanosecond laser flash photolysis (Report 725) or temperature-dependent NMR (Report 388).
    - Hybrid Approach: Use sparse experimental data (e.g., single-timepoint XRD of trapped intermediates) to constrain simulations.
6. Universality Across Derivatives:
    - Parameterize simulations for:
        - Bridge variations (6–14 membered rings).
        - Substituent effects (e.g., $–NO_2$ for redshifted excitation).
    - Unified Output: A "trajectory library" correlating structural features with isomerization rates/quantum yields.

Advantages Over Pure Experiment:

- Atomic Resolution: Reveals hidden intermediates (e.g., twisted or inverted states) undetectable spectroscopically.
- Mechanistic Clarity: Distinguishes rotation vs. inversion pathways (e.g., quantifying bridge strain energy in diazocines).
- Predictive Power: Screens derivatives *in silico* before synthesis (e.g., designing azobenzenes with switch lifetimes >1 ms).

Feasibility Considerations:

- Software: Leverage open-source tools (e.g., Newton-X for TSH, DeePMD for NNP).
- Hardware: Achievable on HPC clusters (~100 GPU-hours per derivative).
- Validation: Experimental partners can provide minimal transient absorption data to

anchor simulations.

This computationally driven approach delivers high-resolution isomerization trajectories at low cost, directly addressing your need for dynamic structural elucidation while leveraging your expertise in bridged systems.

User:

Non-adiabatic or excited-state AIMD is indeed extremely challenging for our HPC systems, but conventional AIMD strategy is definitely usable, without the needs of machine-learning based force fields. Now that we've confirmed that we simulate the Z-E transition trajectories of multiple molecules, sample and extract frames and calculate their vibrational spectra via DFT calculation, there's another question that needs some brainstorming: How to create a predictive framework that predicts real-time structural features of the molecules? There are two immediate questions: What methods should we use for the framework? Are basic neural networks enough, or should we use advanced models like CNNs? What target or targets should we set for prediction?

LLM:

Predictive Framework for Real-Time Structural Feature Prediction from Vibrational Spectra

Core Concept: Develop a multi-output hybrid neural network that maps vibrational spectra to key structural descriptors, enabling real-time monitoring of isomerization dynamics. This addresses the need for a low-cost computational alternative to resource-intensive experiments.

---

1. Methodology Selection: Beyond Basic Neural Networks

While basic NNs (MLPs) can handle spectral regression, 1D Convolutional Neural Networks (1D-CNNs) with attention mechanisms are superior for vibrational spectra due to:

- Spectral Feature Extraction: CNNs excel at capturing local patterns (e.g., peak shifts, broadening) linked to bond/angle changes.
- Attention Mechanisms: Highlight critical spectral regions (e.g., N=N stretch at 1400–1600 cm^{-1}) tied to structural transitions.
- Hybrid Architecture:

graph LR A[Input Spectrum] --> B(1D-CNN for feature extraction) B --> C(Attention Layer weights key bands) C --> D[Fully Connected Branch 1: Geometric Parameters] C --> E[Fully Connected Branch 2: Progress Variable] D --> F[Output: Bond lengths/angles] E --> G[Output: Isomerization state S]

Why not pure MLP? Spectra are high-dimensional (500–2000 data points), and CNNs reduce dimensionality while preserving spatial relationships.

Validation: Benchmark against simpler models (MLP, Random Forest) using simulated spectra→structure pairs.

---

2. Prediction Targets: Focus on Mechanistic Descriptors

Prioritize targets that directly describe the inversion pathway dominant in bridged azobenzenes:

Target Category	Specific Features	Physical Significance
Geometric Parameters	N=N bond length	Shortening indicates transition state (TS) near inversion.
	N-N-C bond angles	Asymmetry distinguishes Z/E states.
	Bridge dihedral angle (e.g., C-N=N-C)	Quantifies ring strain during inversion (critical for diazocines).
Progress Variable (S)	Continuous value [0,1]	0 = pure (E), 1 = pure (Z), 0.5 = TS. Derived from dihedral PCA.
Electronic Descriptor	Partial charge on N atoms	Charge transfer signals TS formation (validated by TD-DFT).

Why these targets?

- They define the reaction coordinate for inversion-dominated isomerization.

- Experimentally inaccessible (e.g., dihedrals) but critical for understanding bridge constraints.

---

3. Data Generation and Training Workflow

1. Simulate Trajectories:
    - Run AIMD for Z→E transitions across 5+ bridged derivatives (vary bridge size/substituents).
    - Sample 10,000+ frames at 10-fs intervals (covers isomerization timescales).
2. Compute Spectra:
    - Generate DFT-level Raman/IR spectra for each frame (ωB97X-D/def2-SVP).
3. Extract Targets:
    - Geometric parameters from AIMD coordinates.
    - Progress variable $S = (\varphi - \varphi\_E)/(\varphi\_Z - \varphi\_E)$, where Φ is key dihedral.
4. Train Hybrid CNN:
    - Input: Spectral vector (500–2000 cm^{-1}, 1-cm^{-1} resolution).
    - Output: 6-8 parameters (bond lengths, angles, S, partial charges).
    - Loss Function: Multi-task weighted MSE (prioritize S and dihedrals).

---

4. Advantages Over Basic Approaches

Method	Strengths	Limitations for This Task
Basic MLP	Fast training	Fails with high-dim spectra; ignores spatial features.
Random Forest	Interpretable	Poor extrapolation to unseen derivatives.
1D-CNN + Attention	Captures spectral structure; generalizable	Higher complexity; requires GPU.

Hybrid CNN Wins: Handles spectral complexity, generalizes across derivatives, and extracts physically meaningful features.

---

5. Validation and Experimental Synergy

- Internal Validation:
    - Train on 4 derivatives, test on the 5th (leave-one-out cross-validation).
    - Compare predicted vs. AIMD-calculated S values (target $R^2 > 0.95$).
- Experimental Anchor Points:
    - Use sparse XRD/NMR data of stable (E) and (Z) states to constrain S endpoints.
    - Validate spectral-structural mapping via steady-state Raman of trapped intermediates.

---

6. Expected Outcomes

- Real-Time Structural Dashboard: Input experimental spectrum → output dynamic structural snapshot.
- Design Rules: Identify bridge geometries that:
    - Maximize isomerization speed (e.g., small dihedral change at TS).
    - Minimize energy barrier (predicted from partial charge shifts).
- Experimental Cost Reduction: Replace 80% of ultrafast experiments with simulation-guided predictions.

This framework transforms vibrational spectra into a window onto molecular dynamics, directly supporting your goals of real-time elucidation for constrained azobenzenes.

User:

The usage of Attention-powered CNN sounds reliable, however there are questions: Since molecular vibrations exist, are individual bond lengths inappropriate for an indication of Z-E transformation? It is not required for the model to predict more than one structural features, and

quality matters more than quantity. And about the progress variable (S), I think it is not as good as using the dihedral angle directly, since it is a processed structural feature that may not reflect that feature accurately. Given our expertise and equipment, Raman spectra is our preferred spectral feature.
LLM:
Refined Predictive Framework: Direct Dihedral Angle Prediction from Raman Spectra
Core Concept: Develop a 1D-CNN with Spectral Attention focused solely on predicting the bridge dihedral angle (e.g., C-N=N-C) from Raman spectra. This prioritizes quality (atomic-resolution accuracy) over quantity, leveraging the dihedral angle as the definitive structural descriptor for inversion-dominated isomerization in bridged azobenzenes.

---

1. Why Dihedral Angle is the Optimal Target
   - Mechanistic Dominance: In bridged systems like diazocines, the dihedral angle directly governs the inversion pathway (Report 687):
     - (E)-isomer: Dihedral ≈ 0° (planar)
     - Transition state: Dihedral ≈ 90° (perpendicular)
     - (Z)-isomer: Dihedral ≈ 180° (twisted)
   - Superiority Over Progress Variable (S):
     - Dihedral is a raw geometric observable (no post-processing needed).
     - Directly correlates with strain energy in bridges (critical for stability).
   - Experimental Relevance: Dihedral changes drive macroscopic properties (e.g., LCST shifts in hydrogels, Report 534).

2. Streamlined Model Architecture: Attention-Based 1D-CNN
Input: Raman spectrum (500–2000 cm^{-1}, $\Delta\nu$ = 1 cm^{-1} → 1501-point vector). Output: Single dihedral angle (e.g., C-N=N-C in degrees).
Architecture:
graph TD A[Raman Spectrum] --> B[1D Convolutional Blocks (Kernels: 5-15 cm^{-1})] B --> C[Attention Layer:
• Self-Attention weights per wavenumber
• Focus on N=N stretch (1420-1480 cm^{-1})
• Penalize irrelevant regions] C --> D[Global Average Pooling] D --> E[Fully Connected Layers (256 → 128 → 64 neurons)] E --> F[Dihedral Angle Output]
Key Design Choices:
   - 1D-CNN: Captures local spectral features (peak shifts/broadening) linked to dihedral changes.
   - Self-Attention Layer: Dynamically weights spectral regions:
     - Prioritizes the N=N stretch region (1420–1480 cm^{-1}) (sensitive to dihedral changes, Report 490).
     - Suppresses noise/low-sensitivity zones (e.g., C-H bends).
   - Why Not Basic MLP?: MLPs fail to exploit spatial relationships in spectra, leading to overfitting.

3. Data Generation & Training Protocol
   1. AIMD Trajectories:
      - Simulate Z→E isomerization for 3–5 bridged derivatives (e.g., diazocine + analogs).
      - Sample frames every 10 fs (~5,000 frames/derivative).
   2. Raman Spectra Calculation:
      - Compute spectra at DFT level (ωB97X-D/def2-SVP; balances accuracy/cost).
      - Include anharmonic corrections for key bands (N=N, bridge modes).
   3. Dihedral Extraction:
      - Calculate C-N=N-C dihedral from atomic coordinates for each frame.
   4. Training:
      - Loss Function: Huber loss (robust to AIMD noise).
      - Regularization: Spectral dropout (randomly mask 5% wavenumbers).
      - Validation: Leave-one-derivative-out cross-validation.

4. Advantages of Dihedral-Centric Approach

Feature	Benefit
Single Output	Eliminates multitask interference → higher accuracy (±2° error achievable).
Physical Interpretability	Attention weights reveal which Raman bands drive predictions (e.g., N=N vs. bridge modes).
Experimental Utility	Predict dihedral from experimental Raman → infer real-time isomerization state.

5. Validation Against Real-World Data
   - Synthetic Benchmarks:
     - Compare predicted dihedrals with AIMD ground truth (target $R^2 > 0.98$).
     - Track attention weights: Verify focus on N=N stretch region.
   - Experimental Anchors:
     - Use XRD/NMR dihedrals of stable (E) and (Z) states as fixed points.
     - Validate with time-resolved Raman of photo-switched samples (nanosecond resolution).
6. Expected Performance & Extensions
   - Accuracy: Dihedral prediction within ±3° (chemically meaningful resolution).
   - Real-Time Application:
     - Input experimental Raman → instant dihedral output → monitor isomerization progress.
     - Example: Dihedral = 90° → transition state population peak.
   - Scalability: Add substituent-insensitive spectral preprocessing (e.g., baseline correction) for broader derivative applicability.

Why This Works for Your Goals:

1. Resource Efficiency:
   - Eliminates costly excited-state MD; uses conventional AIMD + DFT spectra.
   - Model inference requires only a GPU (no HPC).
2. Precision Focus:
   - Dihedral angle is the most sensitive geometric descriptor for bridged azobenzene isomerization.
3. Raman-Centric Design:
   - Attention mechanism tailored to Raman-specific features (e.g., sharp N=N stretch).

This framework delivers a high-fidelity, experimentally actionable predictor for the defining structural feature of your target systems.

Ablation Study: Impact of GraphRAG and model choice

Ablation studies have been done to investigate the impact of RAG being implemented in the interactive research design procedure, whether LLMs demonstrate scientific fidelity without retrieved knowledge. For sessions with RAG disabled, we removed the retrieved knowledge from the interactive design session, kept the rest of system prompt untouched, and sent the initial prompt that started the interactive session. Currently there are three parallel conversation sessions: Session A (DeepSeek R1-0528 with RAG), the one we used in this research, Session B (DeepSeek R1-0528 without RAG) and Session C (Gemini 3 Pro without RAG). Comparing the responses, we observed that GraphRAG noticeably improves the scientific grounding of responses for DeepSeek R1-0528 relative to the no-GraphRAG baseline. DeepSeek R1-0528 responses without GraphRAG exhibited critical scientific mistakes (considering bridged azobenzenes as DHA derivatives, reversing the relationship between N=N stretches in Z- and E- systems). Introducing knowledge retrieved from actual research papers using GraphRAG mitigates such risk and ensure scientifically accurate response. In contrast, Gemini 3 Pro

without GraphRAG generally produced scientifically detailed and coherent responses comparable to, and sometimes stronger than, DeepSeek R1-0528 with GraphRAG. This observation is consistent with the reviewer's point that as base models become more advanced, the marginal benefit of GraphRAG may diminish. Below are raw response from Session B and Session C.

Session B:

Proposed Research Direction:
Development of a Unified Time-Resolved Femtosecond Stimulated Raman Spectroscopy (FSRS) Platform Coupled with Multivariate Analysis for Real-Time Tracking of Z-E Isomerization Dynamics in Bridged Azobenzenes

Rationale and Thought Process:
1. **Problem-Specific Challenges**:
  - Bridged azobenzenes (e.g., DHA derivatives) exhibit constrained inversion-dominated isomerization (unlike rotation in unbridged analogs), leading to unique energy landscapes and transient intermediates.
  - Existing methods (UV-Vis, NMR) lack sufficient temporal resolution (< ps) or molecular specificity to capture ultrafast geometric changes during isomerization.
  - Vibrational spectra (IR/Raman) provide direct structural fingerprints but conventional techniques cannot resolve sub-ps dynamics or disentangle overlapping signals in complex systems.

2. **Core Innovation**:
  - **Femtosecond Stimulated Raman Spectroscopy (FSRS)**:
    - Combines ultrafast temporal resolution (∼50 fs) with high spectral resolution (∼10 cm^{-1}), enabling *real-time tracking* of vibrational mode evolution during isomerization.
    - Probe key vibrations sensitive to N=N bond order (∼1400–1600 cm^{-1}), bridge distortion (∼300–800 cm^{-1}), and phenyl ring deformation (∼1000–1300 cm^{-1}).
  - **Multivariate Kinetic Modeling**:
    - Apply multivariate curve resolution-alternating least squares (MCR-ALS) to FSRS datasets, decomposing spectral evolution into:
      - (a) Pure component spectra (Z, E, transition states)
      - (b) Concentration profiles (kinetic trajectories)
    - Unify analysis across diverse bridged scaffolds by focusing on *universal vibrational markers* (e.g., N=N stretch frequency shift correlated with isomer state).

3. **Methodological Workflow**:
  - **Step 1: Target Synthesis**
    Design DHA-like derivatives with systematic bridge modifications (e.g., ring size, heteroatom substitution) to perturb energy barriers and intermediate stability.
  - **Step 2: FSRS Experiments**
    - Pump (355 nm): Photoinitiate Z→E isomerization.
    - Probe: FSRS captures time-resolved Raman spectra (0–100 ps delays).
    - Control: Compare thermal (slow) vs. photochemical (fast) pathways.
  - **Step 3: Computational Validation**
    - DFT/TD-DFT calculations: Simulate vibrational spectra of ground/excited states and transition geometries.
    - Identify diagnostic modes (e.g., N=N stretch at 1420 cm^{-1} for Z → 1520 cm^{-1} for E).
  - **Step 4: Unified Analysis Framework**
    - Train MCR-ALS models on FSRS data to extract kinetic parameters (rate constants, intermediate lifetimes).
    - Develop a "bridge perturbation index" correlating vibrational shifts with bridge strain energy.

4. **Expected Advantages**:
  - **Real-Time Molecular Movies**: Visualize bond elongation/contraction and bridge distortion dynamics at femtosecond resolution.
  - **Quantitative Universality**: MCR-ALS models transferable to new bridged azobenzenes via shared vibrational descriptors.
  - **Mechanistic Insights**: Resolve contentious pathways (e.g., inversion vs. rotation-assisted inversion) through transient intermediate detection.

5. **Validation & Impact**:
  - Validate against ultrafast X-ray scattering (if accessible) for geometric consistency.
  - Enable rational design of azobenzene-based molecular machines by linking bridge strain to isomerization kinetics.
  - Extend methodology to other photochromic systems (e.g., stiff-stilbenes).

This approach directly addresses your goal by transforming vibrational spectra into a real-time molecular "dashboard" for isomerization dynamics, leveraging the synergy of ultrafast spectroscopy and smart data analysis.

Session 3:

Based on your objectives to systematically investigate bridged azobenzenes (specifically the **dibenzo[c,g][1,2]diazocine** scaffold) and develop a method to map real-time status during Z-E isomerization, I propose the following innovative research direction.

Proposed Research Direction
"4D Spectro-Temporal Mapping: A Machine-Learning Assisted Approach to Decoding the Isomerization Trajectory of Functionalized Diazocines via Time-Resolved Vibrational Spectroscopy."

Executive Summary
This proposal moves beyond standard static characterization (Z vs. E endpoints). Instead, it aims to create a **"Molecular GPS"** that locates exactly where the molecule is on the Potential Energy Surface (PES) at any given moment during the switching process.

By combining High-Throughput Ab Initio Molecular Dynamics (AIMD) with Time-Resolved Infrared (TR-IR) or Raman spectroscopy, we will build a unified predictive model—a "dictionary"—that translates dynamic spectral shifts directly into instantaneous geometric conformations (inversion vs. rotation pathways).

Detailed Research Plan

Phase 1: Systematic Library Expansion (The "Hardware")
The 11,12-Dihydrodibenzo[c,g][1,2]diazocine core is unique because the bridge stabilizes the *Z*-isomer (cis), unlike standard azobenzenes.
* **Action:** Synthesize a systematic library of derivatives with varying substitution patterns at the *para*-positions relative to the azo group (positions 2,3, 8, or 9 on the diazocine core).
* **Variable:** Introduce Push-Pull systems (e.g., Electron Donating Groups on one ring, Electron Withdrawing on the other).
* **Goal:** To modulate the **CNNC dihedral angle** and the height of the rotational energy barrier, thereby creating a diverse set of isomerization speeds and transition state geometries to test the unified method.

Phase 2: The Computational "Digital Twin" (The Unified Method - Part A)
Standard DFT calculates the static endpoints. To understand the *process*, we need dynamics.
* **Action:** Perform **Ab Initio Molecular Dynamics (AIMD)** simulations of the Z-E isomerization on both the excited state (S1, n-π*) and ground state (S0) surfaces.
* **Innovation:** Instead of just calculating energy, you will calculate the **dipole moment autocorrelation function** at intervals along the trajectory. This allows you to generate *theoretical* Vibrational Spectra (IR/Raman) for unstable intermediate species (e.g., the twisted transition state or "phantom" states near the conical intersection) that are impossible to isolate physically.

Phase 3: The "Spectral Decoder" (The Unified Method - Part B)
This is the core innovation satisfying your second objective.
* **Challenge:** Experimental spectra of dynamic processes are often broad and overlapping.
* **Solution:** Train a **Convolutional Neural Network (CNN)** or a Principal Component Analysis (PCA) model using the theoretical data from Phase 2.
  * *Input:* Calculated spectra of transient conformations.
  * *Label:* Exact geometric parameters (CNNC dihedral angle, N=N bond length, Bridge conformation).
* **Result:** You create a "Rosetta Stone" that lets you input an experimental spectrum and output the statistical distribution of molecular geometries.

Phase 4: Experimental Validation
* **Action:** Utilize **Step-Scan FTIR** or **Femtosecond Stimulated Raman Spectroscopy (FSRS)** on the synthesized library.
* **Analysis:** Feed the time-resolved experimental data into the "Spectral Decoder" (Phase 3).
* **Outcome:** You will visualize the real-time "movie" of the bridge flipping and the N=N bond stretching, distinguishing whether the molecule undergoes a volume-conserving "pedal" motion or a bulky "rotation" based purely on the vibrational fingerprint.

Rationale and Thought Process

1. Why this Bridge Type (Diazocines)?
* **Current status:** Standard azobenzenes are well understood. However, diazocines (bridged) are currently the "frontier" because they exhibit **excellent photopharmacological properties** (visible light switching, high quantum yield, thermal stability of the *Z*-form).
* **The Scientific Gap:** The strain imposed by the 8-membered ethylene bridge forces the molecule into a "boat" or "chair" conformation. It is currently debated how exactly the strain energy relaxes during isomerization. Does the bridge "breathe" first, or does the N=N bond twist first? Your systematic research will answer this.

2. Why Vibrational Spectroscopy (IR/Raman) over UV-Vis?
* **UV-Vis** is broad and relies on electronic transitions; it tells you *electronic* state populations (S0 vs S1) but is structurally blind.
* **Vibrational Spectroscopy** provides a "structural fingerprint." The N=N stretching frequency (approx. 1400-1500 cm^{-1}) and the C-N stretch are highly sensitive to bond order and the N-N bond length. Specifically, the "breathing" modes of the 8-membered ring in the fingerprint region (600-1000 cm^{-1}) will act as a reporter for the strain status of the bridge.

3. Why the "Unified Method" incorporating Machine Learning?
* **The User's Constraint:** You asked to elucidate "real-time status... from observable

information."
* **The Problem:** In a dynamic process, the observable signal is an ensemble average of millions of molecules, some in the Z-state, some in the E-state, and some in the Transition State. Human analysis cannot deconstruct a broad spectral peak into these components accurately.
* **The Innovation:** By computationally generating the spectra of the *intermediates* and using ML to recognize these patterns in experimental data, you bridge the gap between "what we see" (spectrum) and "what is happening" (molecular distinct geometry).

Expected Impact
This approach transforms the definition of "characterization" in azobenzene chemistry. Instead of reporting "Molecule X switches in 10 picoseconds," you will report "Molecule X switches via a synchronized pedal motion where the bridge relaxation precedes the N=N inversion by 200 femtoseconds." This level of mechanistic detail is crucial for designing next-generation molecular switches for data storage and artificial muscle applications.

References

1. VandeVondele, J. et al., Quickstep: Fast and accurate density functional calculations using a mixed Gaussian and plane waves approach. *Comput. Phys. Commun.* **167**, 103-128 (2005).

2. Perdew, J. P., Burke, K., & Ernzerhof, M. Generalized gradient approximation made simple. *Phys. Rev. Lett.* **77**, 3865-3868 (1996).

3. Grimme, S., Antony, J., Ehrlich, S., & Krieg, H. A consistent and accurate ab initio parametrization of density functional dispersion correction (DFT-D) for the 94 elements H-Pu. *J. Chem. Phys.* **132**, 154104 (2010).

4. VandeVondele, J. & Hutter, J. Gaussian basis sets for accurate calculations on molecular systems in gas and condensed phases. *J. Chem. Phys.* **127** (2007).

5. Barducci, A., Bussi, G., & Parrinello, M. Well-tempered metadynamics: a smoothly converging and tunable free-energy method. *Phys. Rev. Lett.* **100**, 020603 (2008).

6. Nosé, S. Constant Temperature Molecular Dynamics Methods. *Prog. Theor. Phys. Suppl.* **103**, 1-46 (1991).

7. Lu, T. & Chen, F. Multiwfn: A multifunctional wavefunction analyzer. *J. Comput. Chem.* **33**, 580-592 (2012).

8. Samanta, S., Qin, C., Lough, A. J., & Woolley, G. A. Bidirectional photocontrol of peptide conformation with a bridged azobenzene derivative. *Angew. Chem. Int. Ed. Engl.* **51**, 6452-6455 (2012).

9. Cabré, G. et al. Synthetic photoswitchable neurotransmitters based on bridged azobenzenes. *Org. lett.* **21**, 3780-3784 (2019).

10. S. Li, G. Han, W. Zhang, Concise synthesis of photoresponsive polyureas containing bridged azobenzenes as visible-light-driven actuators and reversible photopatterning. *Macromol.* **51**, 4290-4297 (2018).

11. Zhou, H. et al. Bridged Azobenzene Enables Dynamic Control of Through-Space Charge Transfer for Photochemical Conversion. *J. Phys. Chem. Lett.* **12**, 3868-3874 (2021).

12. Lentes, P. et al. Nitrogen bridged diazocines: Photochromes switching within the near-infrared region with high quantum yields in organic solvents and in water. *J. Am. Chem. Soc.* **141**, 13592-13600 (2019).

13. Maier, M. S. et al. Oxidative Approach Enables Efficient Access to Cyclic Azobenzenes. *J. Am. Chem. Soc.* **141**, 17295−17304 (2019).